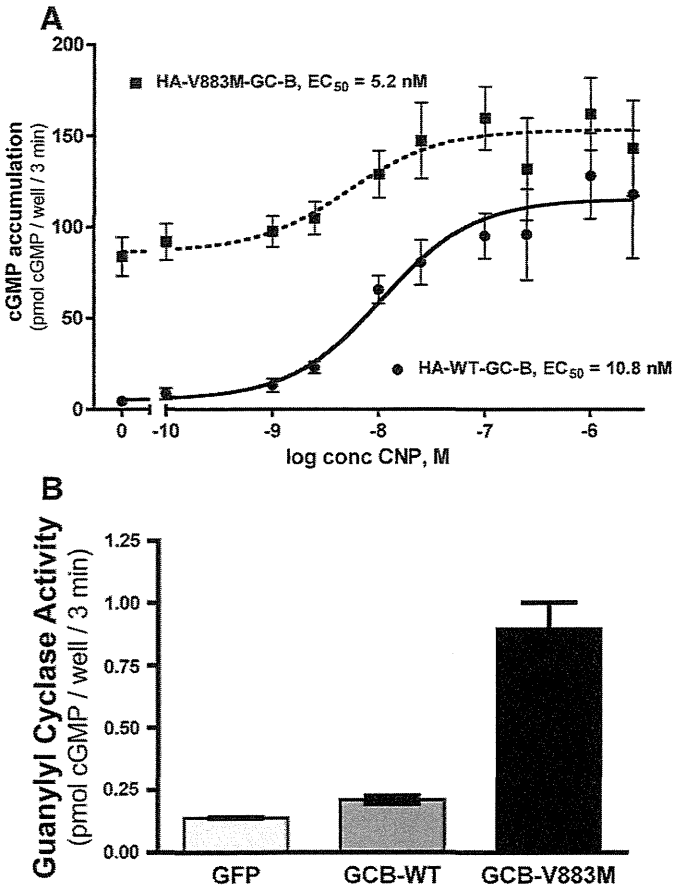

Fig. 1. Basal cGMP concentrations are markedly elevated in cells expressing V883M-GC-B. A, 293 cells transiently expressing HA-WT-GC-B or HA-V883M-GC-B were incubated with the indicated concentrations of CNP for 3 min and then intracellular cGMP concentrations were determined. The EC_{50}s for the two enzymes were not significantly different, $p = 0.42$. B, ATDC5 cells were transiently transfected with plasmids expressing WT-GC-B or GC-B-V883M and cGMP concentrations were measured in basal (no CNP) serum-starved cells 2 days later. Cyclic GMP concentrations in cells expressing WT-GC-B were slightly higher than those observed in un-transfected cells ($p < 0.01$), but levels in cells expressing GC-B-V883M were 4.3-fold higher than those in cells expressing WT-GC-B ($p < 0.03$).

HA-WT-GC-B or HA-V883M-GC-B under basal (1 mM Mg^{2+}GTP), hormone-stimulated (1 mM Mg^{2+}GTP, 1 mM ATP and 1 μM CNP), or detergent-stimulated (1 mM Mn^{2+}GTP and 1% Triton X-100) condition (Fig. 2). Enzyme analysis was performed in the 293 cells because they do not express detectable endogenous GC activity [6], which allows more definitive interpretation of the data because most tissues and cell lines express more than one GC.

GC activity measured in crude membranes from GFP transfected cells was insignificant under all conditions. Consistent with the whole cell cGMP analysis describe in Fig. 1, basal GC activity was low for WT-GC-B and HA-WT-GC-B but was elevated 28-fold over WT levels for HA-V883M-GC-B. Saturating concentrations of CNP and ATP stimulated WT-GC-B and HA-WT-GC-B similarly (>50-fold). However, GC activity of HA-WT-GC-B was almost double that of the WT enzyme lacking the HA tag, consistent with higher expression of the HA-tagged receptor. As in whole cells, CNP and ATP activated HA-V883M-GC-B about two-fold in enzyme assays. GC activity of HA-V883M-GC-B measured in the presence of detergent was lower than that observed for HA-WT-GC-B, which is consistent with reduced expression of HA-V883M-GC-B compared to HA-WT-GC-B. Western analysis of SDS-PAGE fractionated immunoprecipitated enzymes confirmed that the more slowly migrating, completely processed species (upper band) was expressed at lower levels than the comparably processed forms of the tagged or untagged WT version of GC-B (Fig. 2, inset). We previously

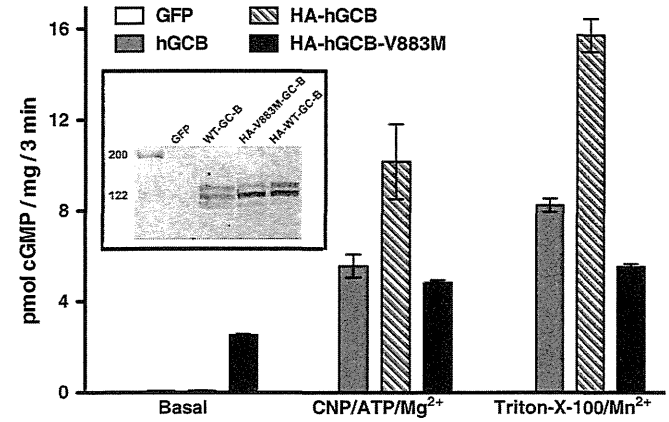

Fig. 2. GC activity but not the protein level of V883M-GC-B was elevated in the absence of CNP. Crude membranes from 293 cells transfected with plasmids expressing the indicated constructs were assayed for GC activity under the conditions indicated in the figure legend and text. Bars within the symbols indicate the range of duplicate determinations. This figure is representative of two independent assays. The inset shows a Western blot of the indicated forms of GC-B purified from 293 cells transiently transfected with the indicated constructs. The numbers on the left indicate the molecular weight of standards.

demonstrated that only the upper band of GC-B is phosphorylated and that phosphorylation is required for CNP-dependent activation of GC-B [8,29].

Maximal velocity of HA-GC-B-V883M is elevated

To determine how the mutation increased the enzymatic activity of GC-B, substrate–velocity curves were generated for HA-WT-GC-B and HA-V883M-GC-B with or without 1 μM CNP in the absence of ATP (Fig. 3A). Basal activity of the WT enzyme was low and CNP increased Vmax 12-fold without decreasing the Km. Consistent with previous observations [6], WT-GC-B was positive cooperative as indicated by a Hill slope of 1.3. In contrast, basal maximal velocity of the mutant enzyme was elevated 15-fold compared to WT-GC-B and the Km was unchanged. The Hill coefficient was 0.9, suggesting slight negative cooperativity. CNP failed to increase the maximal velocity of HA-V883M-GC-B, but reduced the Hill slope 0.4 units and the Km 10-fold. Thus, the V883M mutation increases basal maximal velocity, reduces the Hill coefficient and allows CNP to reduce the Km in the absence of ATP. In contrast, the reduction in Hill coefficient and Km for the WT enzyme was previously shown to be completely dependent on the presence of ATP [5]. These data are consistent with the V883M mutation producing a structural change in GC-B that locks it into a conformation that mimics that of the ATP-bound state. They also indicate for the first time that the CNP-dependent changes in the Vmax and Km of GC-B are separate but related processes.

CNP reduces the Hill coefficient and Km of HA-V883M-GC-B in a concentration-dependent manner in the absence of ATP

Substrate–velocity curves were generated for HA-V883M-GC-B in the presence of increasing concentrations of CNP to evaluate the concentration-dependence of CNP on reductions in the Hill coefficient and Michaelis constant (Fig. 3B). ATP was not included in these experiments. In the absence of CNP, no cooperativity was observed, but increasing concentrations of CNP progressively increased the amount of negative cooperativity while concomitantly decreasing the Km. These data indicate that CNP converts HA-V883M-GC-B to a strongly negative cooperative enzyme. Similarly, in the absence of CNP, the Km of the mutant enzyme was high; but in the presence of increasing concentrations of CNP, the Km dropped progressively while maximal velocity was unaffected.

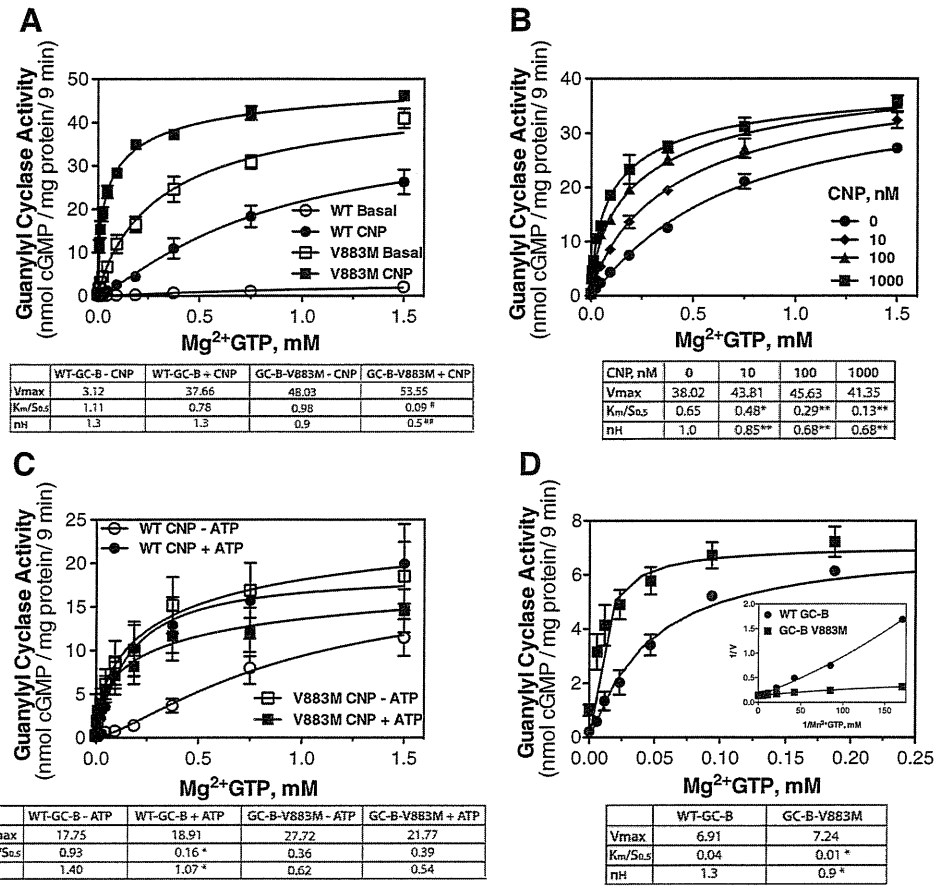

	WT-GC-B - CNP	WT-GC-B + CNP	GC-B-V883M - CNP	GC-B-V883M + CNP
Vmax	3.12	37.66	48.03	53.55
Km/So.5	1.11	0.78	0.98	0.09 #
nH	1.3	1.3	0.9	0.5 ##

CNP, nM	0	10	100	1000
Vmax	38.02	43.81	45.63	41.35
Km/So.5	0.65	0.48*	0.29**	0.13**
nH	1.0	0.85**	0.68**	0.68**

	WT-GC-B - ATP	WT-GC-B + ATP	GC-B-V883M - ATP	GC-B-V883M + ATP
Vmax	17.75	18.91	27.72	21.77
Km/So.5	0.93	0.16 *	0.36	0.39
nH	1.40	1.07 *	0.62	0.54

	WT-GC-B	GC-B-V883M
Vmax	6.91	7.24
Km/So.5	0.04	0.01 *
nH	1.3	0.9 *

Fig. 3. Kinetic characterization of V883M-GC-B. GC activity shown in panels A–D was measured for 9 min in crude membranes from 293 cells transiently expressing either HA-GC-B-WT or HA-GC-B-V883M. Bars within symbols indicate the SEM. Tables below each figure show Vmax, Km and Hill coefficient (n_H). A. Maximal velocity of HA-V883M-GC-B is elevated in the absence of CNP. GC activity was measured in the presence or absence of 1 μM CNP and the indicated concentrations of Mg^{2+}GTP where n = 4. The # indicates a significant difference from HA-WT-GC-B-CNP at $p < 0.05$. The ## indicates a significant difference from HA-V883M-GC-B-CNP at $p < 0.03$. B. CNP decreases the Hill coefficient and Km for HA-V883M-GC-B in a concentration-dependent manner in the absence of ATP. GC activity was measured in the presence or absence of increasing concentrations of CNP and the indicated concentrations of Mg^{2+}GTP where n = 4. * and ** indicate a significant difference from no CNP values where $p < 0.05$ and 0.01, respectively. C. ATP does not affect the Hill coefficient or Km of HA-V883M-GC-B. GC activity was measured in the presence or absence of 0.1 mM ATP, 1 μM CNP and the indicated concentrations of Mg^{2+}GTP where n = 4. The * indicates a significant difference from HA-WT-GC-B (−) ATP at $p < 0.05$. D. HA-V883M-GC-B is negative cooperative. GC activity was measured with the indicated concentrations of Mn^{2+}GTP and 1% Triton X-100 where n = 6. The * indicates a significant difference from the corresponding value obtained for the WT enzyme at $p < 0.05$; inset. Double reciprocal plots were generated from the raw data to demonstrate a concave upward curve indicative of positive cooperativity or a slightly downward curve indicative of negative cooperativity.

ATP does not allosterically activate V883M-GC-B

We recently determined that CNP reduces the Hill coefficient and Km of WT-GC-B by a process that requires ATP binding to an allosteric site in the catalytic domain [6]. Therefore, we investigated whether the V883M mutation affected these processes as well. Substrate–velocity curves were generated for HA-WT-GC-B and HA-V883M-GC-B in the presence of 1 μM CNP with or without 0.1 mM ATP. With the WT enzyme, ATP reduced the Km 6-fold and the Hill coefficient 0.3 units without affecting the Vmax (Fig. 3C). However, ATP failed to reduce the Km or Hill coefficient or increase the Vmax of HA-V883M-GC-B. These data are consistent with a scenario where the V883M mutation causes a conformational change in GC-B that abolishes the need for ATP in the CNP-dependent reduction in Hill coefficient and Km.

HA-V883M-GC-B is slightly negative cooperative when manganese is used as a cofactor

Substrate–velocity curves were also generated on membranes expressing HA-WT-GC-B or HA-V883M-GC-B under non-physiologic, detergent conditions using manganese-GTP as substrate (Fig. 3D). Substrate–velocity curves generated under these conditions were previously shown to be positive cooperative for GC-A [37]. Vmax was lower when measured under these conditions but the Km/S0.5 was strikingly lower compared to physiologic activation conditions. Maximal velocity was not different between the WT and mutant GC-B enzymes. The substrate–velocity curve for HA-WT-GC-B was positive cooperative as demonstrated by concave upward reciprocal plots and a Hill coefficient of 1.3 (Fig. 3D, inset). To our knowledge, this is the first demonstration of positive cooperativity for GC-B when assayed under detergent-stimulated conditions. In contrast to HA-WT-GC-B, HA-V883M-GC-B was weakly negative cooperative as indicated by a slightly concave downward curve and a Hill coefficient of 0.9 (Fig. 3D, inset), which is consistent with the slight negative cooperativity observed for V883-GC-B when assayed under basal conditions.

HA-V883M-GC-B is resistant to desensitization

Cyclic GMP concentrations in cells expressing V883M-GC-B were highly elevated two days after transfection (Fig. 1), which suggests that the mutant enzyme was not completely desensitized or downregulated. In contrast, CNP activated WT-GC-B was shown to desensitize in less than one hour [8]. Therefore, we examined whether the V883M mutation disrupted the inactivation of GC-B.

GC activity was measured on membranes from cells expressing HA-WT-GC-B or HA-V883M-GC-B for up to 2 h to evaluate the effect of the V883M mutation on the inactivation of GC-B as a function of time (Fig. 4, top panel). WT GC activity was determined in the

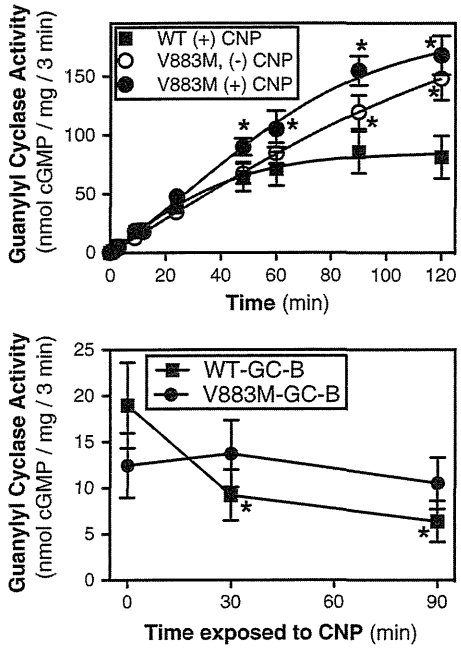

Fig. 4. V883M-GC-B is resistant to desensitization. A. GC assays were conducted on crude membranes from 293 cells transfected with HA-WT-GC-B or HA-V883M-GC-B for the period of time indicated in the presence of 1 mM GTP, 1 mM ATP and 5 mM $Mg^{2+}Cl_2$ with or without 1 μM CNP. Each value represents 4 determinations. The asterisks indicate a significant difference from corresponding values obtained in membranes expressing WT-GC-B at $p < 0.02$. B. Whole 293 cells transfected with HA-WT-GC-B or HA-V883M-GC-B were incubated with 1 μM CNP for the indicated times. Membranes were then prepared and assayed for GC activity in the presence of 1 mM GTP, 1 mM ATP and 5 mM $Mg^{2+}Cl_2$. N = 4. The asterisks indicate significance from the 0 time point value where $p < 0.05$. The bars within the symbols indicate SEM in all panels.

presence of CNP, whereas mutant activity was determined in the presence and absence of CNP. The GC activity of the WT enzyme declined with time and was inactive after 60 min. In contrast, the GC activity of the mutant receptor was linear for the duration of the assay regardless of whether CNP was included in the assay.

We also examined the inactivation of the WT and mutant enzymes under whole cell conditions. In this experiment, intact cells were treated with 1 μM CNP for 0, 30 or 90 min then membranes were prepared from the cells and assayed for GC activity for 3 min (Fig. 4, bottom panel). The WT enzyme demonstrated a time-dependent inactivation similar to that previously reported for GC-B expressed in 3T3 cells [8]. However, exposure of the V883M-GC-B to saturating concentrations of CNP failed to inactivate the enzyme after 30 or 90 min. Together, these data indicate that the Val substitution at position 883 not only increases the maximal velocity of the enzyme, it also disrupts the normal desensitization process.

Activation of GC-B by the V883M substitution does not require phosphorylation

CNP only activated a GC-B construct containing alanine substitutions for the first six phosphorylation sites identified in GC-B (S513, T516, S518, S523, S526, T529) two-fold as opposed to greater than 30-fold for WT-GC-B [29], whereas the analogous substitutions left GC-A completely unresponsive to NP stimulation [38]. These observations led to the idea that phosphorylation is required for NP-dependent activation of GC-A and GC-B. Here, we asked whether phosphorylation is also required for the V883M mutation to increase GC-B activity.

To do this, we mutated Val-883 to Met in the rat GC-B-7A construct that contains alanine substitutions for the first six identified sites plus Ser-522, which is not phosphorylated [29]. We also created a constitutively phosphorylated mimetic version of rat GC-B-V883M by mutating Val-883 to Met in GC-B-7E. Rat GC-B-7E contains glutamate substitutions for the first six identified sites as well as Ser-489, a newly identified putative site that reduces the Km of GC-B when phosphorylated [30].

Introducing the Val-883–Met mutation into WT-GC-B increased basal activity 39-fold, whereas the same mutation in the dephosphorylated form of the enzyme (GC-B-7A) increased activity 17-fold (Fig. 5). However, introduction of the V883M mutation into the GC-B-7E construct increased activity 68-fold. Thus, phosphorylation is not required for the elevated basal activity associated with the V883M mutation, but phosphorylation results in greater activation since the WT and phosphorylation mimetic enzymes (GC-B-7E) were activated to a greater degree than the non-phosphorylated enzyme (GC-B-7A).

Discussion

Characterization of the missense mutant revealed several important changes in GC-B that occurred as a result of this single amino acid substitution. First, basal maximal velocity was dramatically increased. Second, the CNP-dependent reduction in Km was rendered independent of ATP, and thirdly, the normal desensitization process was inactivated. Another worthy point of discussion is that the V883M-GC-B mutant is the first example of a GC where ligand binding reduces the Km without increasing maximal velocity. Thus, the kinetic analysis of this mutant allowed the separation of the maximal velocity increasing effects of ligand binding from the Km reducing effects of ligand binding for the first time. This mutant enzyme also provides unequivocal support for the new GC-B activation model where CNP binding increases activity by reducing the Km as well as increasing maximal velocity [6].

Early studies indicated that product formation by membrane GCs in the presence of detergent is positive cooperative [39,40]. We found that GC-B is positive cooperative under basal conditions as well as when assayed in the presence of $Mn^{2+}GTP$ and Triton X-100. However, the single V883M mutation converts the enzyme from positive cooperative to slightly negative cooperative when assayed under both physiologic and detergent-activated conditions. Interestingly, CNP increased the degree of negative cooperativity of V883M-GC-B in a concentration-dependent manner.

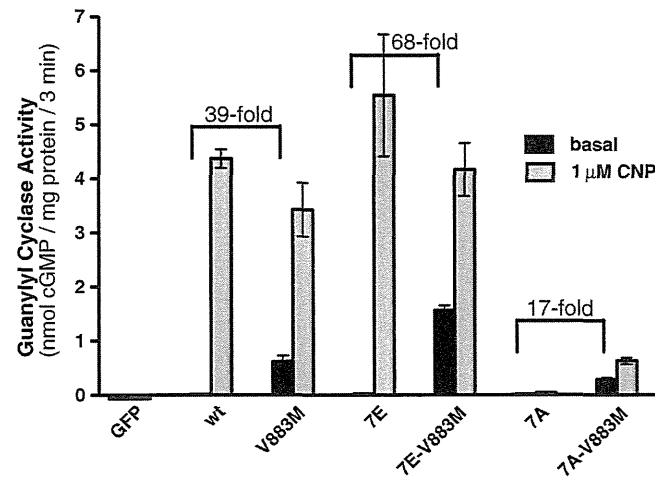

Fig. 5. The GC-B-V883M mutation activates a dephosphorylated version of GC-B. The V883M mutation was introduced into WT-GC-B, constitutively phosphorylated (7E) or constitutively dephosphorylated (7A) forms of GC-B. 293 cells were transiently transfected with plasmids expressing the indicated GC-B constructs. GC assays were performed for 3 min in the presence of 0.1 mM GTP, 1 mM ATP and 5 mM $Mg^{2+}Cl_2$ with or without 1 μM CNP. Each value represents 6 determinations. The bars within the symbols indicate SEM. The values above the brackets indicate the fold-difference above basal values.

The reduction in Km and increase in negative cooperativity appear paradoxical. We hypothesize that the V883M mutant locks the enzyme into a conformation that mimics an ATP bound state. This hypothesis is supported by low or no cooperativity under basal conditions and the inability of ATP to change the activity of the mutant enzyme. In addition, CNP alone markedly decreased the Km of GC-B-V883M, a phenomenon that requires ATP with the WT enzyme. Since cooperativity is maintained, this suggests that the mutation does not destroy the ability of GTP to bind to the allosteric site but rather modifies how GTP binding to the allosteric site affects the catalytic site. However, an alternative

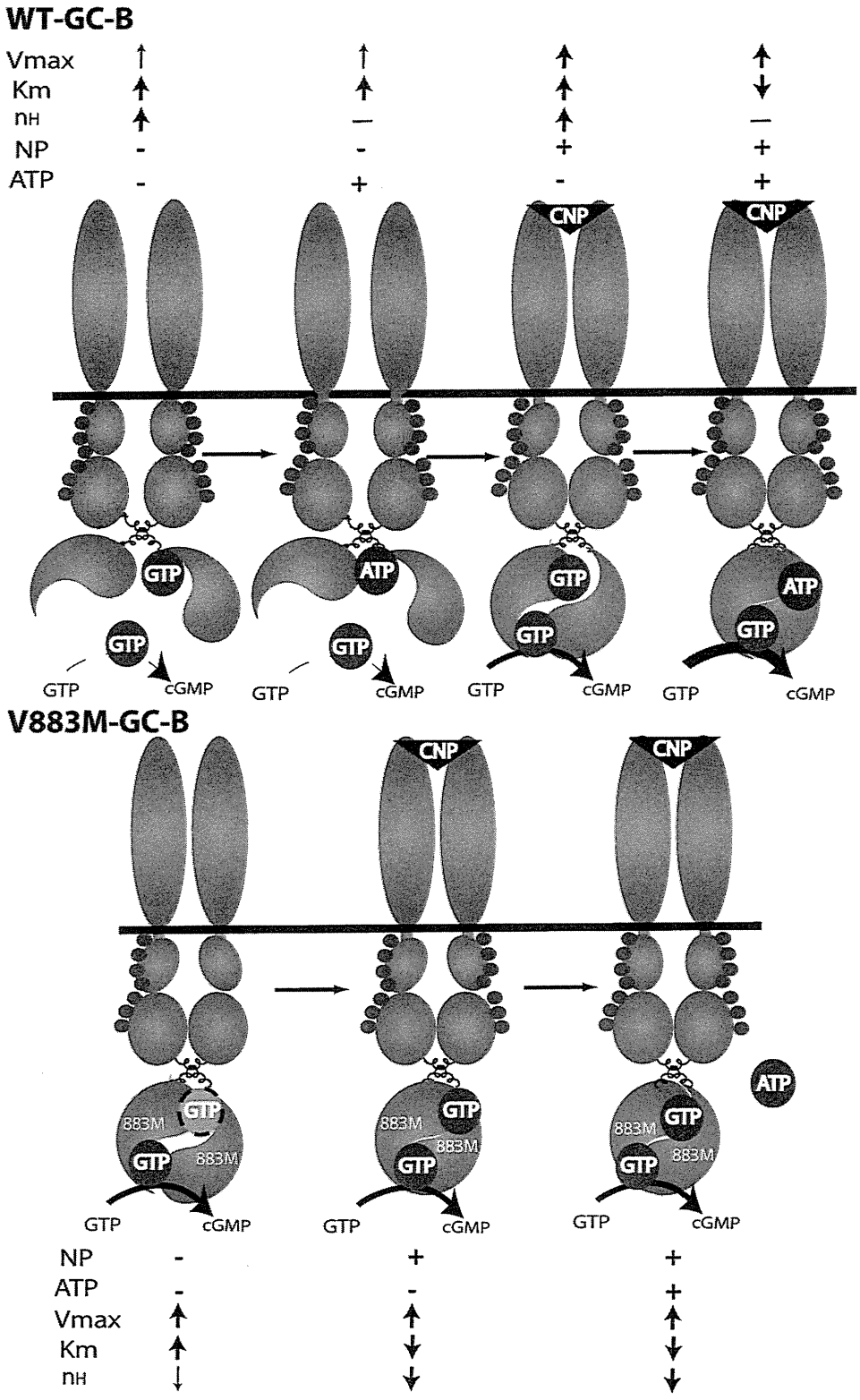

Fig. 6. Activation models for wild type and mutant GC-B. The models are described in detail under the Discussion section. The blue spheres indicate known phosphorylation sites in the kinase homology domain of GC-B. The white 883M indicates that the Val to Met mutation is in the catalytic domain. The abbreviations are: CNP, C-type natriuretic peptide; Km, Michaelis constant; n_H, Hill coefficient; and Vmax, maximal velocity.

explanation is that the reduction in the Hill coefficient results from increased inhibition resulting from GTP binding to a site independent of the allosteric site. This third GTP binding site would explain the appearance of negative cooperativity while also allowing for the Km reduction resulting from the previously identified allosteric site. It is also possible that the V883M mutation could increase the affinity of GC-B for the products of the reaction (pyrophosphate and cGMP), which would result in reduced GC activity and apparent negative cooperativity. Importantly, since the V883M mutation did not affect Vmax when measured in the presence of detergent and manganese, it suggests that the mutation modifies the conformation of the active site under physiologic conditions and does not directly interact with the substrate.

Near linear cGMP production with time by HA-V883M-GC-B assayed both in the presence and absence of CNP indicated that HA-V883M-GC-B is resistant to desensitization. Experiments with alanine and glutamate substituted receptors indicated that unlike CNP activation of WT-GC-B, the increased activity observed with the V883M mutation does not require phosphorylation of the kinase homology domain, although activation was greater with the phosphorylated and phosphomimetic enzymes. The lack of dependence on phosphorylation for activity of the mutant enzyme may contribute to its resistance to desensitization.

It is surprising how much the single amino acid substitution changes the regulation of GC-B (Fig. 6). In the absence of CNP and ATP, maximal velocity of WT-GC-B was low, affinity for substrate was low (high Km), and cooperative was significant and positive. In contrast, under the same conditions, maximal velocity of V883M-GC-B was high, affinity for substrate was low, and cooperativity was low and negative. Addition of ATP in the absence of CNP abolished positive cooperativity of the WT enzyme due to ATP replacing GTP at the allosteric site [6], but had no effect on the mutant enzyme under identical conditions. CNP alone increased maximal velocity of the WT enzyme, but it did not decrease the Km in the absence of ATP. In contrast, CNP alone failed to increase maximal velocity of the mutant enzyme but decreased the Km ten-fold in the absence of ATP. Finally, CNP reduced the cooperativity of both enzymes, but the WT enzyme went from positive to no cooperativity, whereas the mutant went from slightly negative cooperative to very negative cooperative.

In conclusion, we established a molecular mechanism for how a single amino acid substitution in GC-B activates the enzyme, which results in abnormally long and fragile human bones. It will be interesting to determine the prevalence of this mutation in humans and other species.

Conflict of interest statement

None of the authors have a conflict of interest associated with this study.

Acknowledgments

Grant-in Aid (21,922) from the University of Minnesota Graduate School to LRP and the National Institute of Arthritis and Musculoskeletal and Skin Diseases Training Grant T32AR050938 to JWR supported this work.

References

[1] Tamura N, Doolittle LK, Hammer RE, Shelton JM, Richardson JA, Garbers DL. Critical roles of the guanylyl cyclase B receptor in endochondral ossification and development of female reproductive organs. Proc Natl Acad Sci U S A 2004;101:17300–5.
[2] Schmidt H, Stonkute A, Juttner R, Schaffer S, Buttgereit J, Feil R, et al. The receptor guanylyl cyclase Npr2 is essential for sensory axon bifurcation within the spinal cord. J Cell Biol 2007;179:331–40.
[3] Zhang M, Su YQ, Sugiura K, Xia G, Eppig JJ. Granulosa cell ligand NPPC and its receptor NPR2 maintain meiotic arrest in mouse oocytes. Science 2010;330:366–9.
[4] Potter LR, Hunter T. Guanylyl cyclase-linked natriuretic peptide receptors: structure and regulation. J Biol Chem 2001;276:6057–60.
[5] Antos LK, Potter LR. Adenine nucleotides decrease the apparent Km of endogenous natriuretic peptide receptors for GTP. Am J Physiol Endocrinol Metab 2007;293:E1756–63.
[6] Robinson JW, Potter LR. Guanylyl cyclases A and B are asymmetric dimers that are allosterically activated by ATP binding to the catalytic domain. Sci Signal 2012;5:ra65.
[7] Duda T, Goraczniak RM, Sitaramayya A, Sharma RK. Cloning and expression of an ATP-regulated human retina C-type natriuretic factor receptor guanylate cyclase. Biochemistry 1993;32:1391–5.
[8] Potter LR. Phosphorylation-dependent regulation of the guanylyl cyclase-linked natriuretic peptide receptor B: dephosphorylation is a mechanism of desensitization. Biochemistry 1998;37:2422–9.
[9] Hagiwara H, Sakaguchi H, Itakura M, Yoshimoto T, Furuya M, Tanaka S, et al. Autocrine regulation of rat chondrocyte proliferation by natriuretic peptide C and its receptor, natriuretic peptide receptor-B. J Biol Chem 1994;269:10729–33.
[10] Suda M, Ogawa Y, Tanaka K, Tamura N, Yasoda A, Takigawa T, et al. Skeletal overgrowth in transgenic mice that overexpress brain natriuretic peptide. Proc Natl Acad Sci U S A 1998;95:2337–42.
[11] Krejci P, Masri B, Fontaine V, Mekikian PB, Weis M, Prats H, et al. Interaction of fibroblast growth factor and C-natriuretic peptide signaling in regulation of chondrocyte proliferation and extracellular matrix homeostasis. J Cell Sci 2005;118:5089–100.
[12] Woods A, Khan S, Beier F. C-type natriuretic peptide regulates cellular condensation and glycosaminoglycan synthesis during chondrogenesis. Endocrinology 2007;148:5030–41.
[13] Chusho H, Tamura N, Ogawa Y, Yasoda A, Suda M, Miyazawa T, et al. Dwarfism and early death in mice lacking C-type natriuretic peptide. Proc Natl Acad Sci U S A 2001;98:4016–21.
[14] Tamura N, Garbers DL. Regulation of the guanylyl cyclase-B receptor by alternative splicing. J Biol Chem 2003;278:48880–9.
[15] Jaubert J, Jaubert F, Martin N, Washburn LL, Lee BK, Eicher EM, et al. Three new allelic mouse mutations that cause skeletal overgrowth involve the natriuretic peptide receptor C gene (Npr3). Proc Natl Acad Sci U S A 1999;96:10278–83.
[16] Matsukawa N, Grzesik WJ, Takahashi N, Pandey KN, Pang S, Yamauchi M, et al. The natriuretic peptide clearance receptor locally modulates the physiological effects of the natriuretic peptide system. Proc Natl Acad Sci U S A 1999;96:7403–8.
[17] Tamura N, Ogawa Y, Chusho H, Nakamura K, Nakao K, Suda M, et al. Cardiac fibrosis in mice lacking brain natriuretic peptide. Proc Natl Acad Sci U S A 2000;97:4239–44.
[18] Kake T, Kitamura H, Adachi Y, Yoshioka T, Watanabe T, Matsushita H, et al. Chronically elevated plasma C-type natriuretic peptide level stimulates skeletal growth in transgenic mice. Am J Physiol Endocrinol Metab 2009;297:E1339–48.
[19] Lorget F, Kaci N, Peng J, Benoist-Lasselin C, Mugniery E, Oppeneer T, et al. Evaluation of the therapeutic potential of a CNP analog in a Fgfr3 mouse model recapitulating achondroplasia. Am J Hum Genet 2012;91:1108–14.
[20] Yasoda A, Kitamura H, Fujii T, Kondo E, Murao N, Miura M, et al. Systemic administration of C-type natriuretic peptide as a novel therapeutic strategy for skeletal dysplasias. Endocrinology 2009;150:3138–44.
[21] Bartels CF, Bukulmez H, Padayatti P, Rhee DK, van Ravenswaaij-Arts C, Pauli RM, et al. Mutations in the transmembrane natriuretic peptide receptor NPR-B impair skeletal growth and cause acromesomelic dysplasia, type Maroteaux. Am J Hum Genet 2004;75:27–34.
[22] Hachiya R, Ohashi Y, Kamei Y, Suganami T, Mochizuki H, Mitsui N, et al. Intact kinase homology domain of natriuretic peptide receptor-B is essential for skeletal development. J Clin Endocrinol Metab 2007;92:4009–14.
[23] Khan S, Hussain Ali R, Abbasi S, Nawaz M, Muhammad N, Ahmad W. Novel mutations in natriuretic peptide receptor-2 gene underlie acromesomelic dysplasia, type Maroteaux. BMC Med Genet 2012;13:44.
[24] Olney RC, Bukulmez H, Bartels CF, Prickett TC, Espiner EA, Potter LR, et al. Heterozygous mutations in natriuretic peptide receptor-B (NPR2) are associated with short stature. J Clin Endocrinol Metab 2006;91:1229–32.
[25] Bocciardi R, Ravazzolo R. C-type natriuretic peptide and overgrowth. Endocr Dev 2009;14:61–6.
[26] Moncla A, Missirian C, Cacciagli P, Balzamo E, Legeai-Mallet L, Jouve JL, et al. A cluster of translocation breakpoints in 2q37 is associated with overexpression of NPPC in patients with a similar overgrowth phenotype. Hum Mutat 2007;12:1183–8.
[27] Estrada K, Krawczak M, Schreiber S, van Duijn K, Stolk L, van Meurs JB, et al. A genome-wide association study of northwestern Europeans involves the C-type natriuretic peptide signaling pathway in the etiology of human height variation. Hum Mol Genet 2009;18:3516–24.
[28] Miura K, Namba N, Fujiwara M, Ohata Y, Ishida H, Kitaoka T, et al. An overgrowth disorder associated with excessive production of cGMP due to a gain-of-function mutation of the natriuretic peptide receptor 2 gene. PLoS One 2012;7:e42180.
[29] Potter LR, Hunter T. Identification and characterization of the major phosphorylation sites of the B-type natriuretic peptide receptor. J Biol Chem 1998;273:15533–9.
[30] Yoder AR, Robinson JW, Dickey DM, Andersland J, Rose BA, Stone MD, et al. A functional screen provides evidence for a conserved, regulatory, juxtamembrane phosphorylation site in guanylyl cyclase A and B. PLoS One 2012;7:e36747.
[31] Dickey DM, Burnett Jr JC, Potter LR. Novel bifunctional natriuretic peptides as potential therapeutics. J Biol Chem 2008;283:35003–9.
[32] Bryan PM, Potter LR. The atrial natriuretic peptide receptor (NPR-A/GC-A) is dephosphorylated by distinct microcystin-sensitive and magnesium-dependent protein phosphatases. J Biol Chem 2002;277:16041–7.
[33] Robinson JW, Potter LR. ATP potentiates competitive inhibition of guanylyl cyclase A and B by the staurosporine analog, Go6976: reciprocal regulation of ATP and GTP binding. J Biol Chem 2011;286:33841–4.
[34] Abbey-Hosch SE, Smirnov D, Potter LR. Differential regulation of NPR-B/GC-B by protein kinase C and calcium. Biochem Pharmacol 2005;70:686–94.

[35] Flora DR, Potter LR. Prolonged atrial natriuretic peptide exposure stimulates guanylyl cyclase-A degradation. Endocrinology 2010;151:2769–76.
[36] Fujishige K, Kotera J, Yanaka N, Akatsuka H, Omori K. Alteration of cGMP metabolism during chondrogenic differentiation of chondroprogenitor-like EC cells, ATDC5. Biochim Biophys Acta 1999;1452:219–27.
[37] Ivanova K, Heim JM, Gerzer R. Kinetic characterization of atrial natriuretic factor-sensitive particulate guanylate cyclase. Eur J Pharmacol 1990;189:317–26.
[38] Potter LR, Hunter T. Phosphorylation of the kinase homology domain is essential for activation of the A-type natriuretic peptide receptor. Mol Cell Biol 1998;18: 2164–72.
[39] Chrisman TD, Garbers DL, Parks MA, Hardman JG. Characterization of particulate and soluble guanylate cyclases from rat lung. J Biol Chem 1975;250:374–81.
[40] Kimura H, Murad F. Evidence for two different forms of guanylate cyclase in rat heart. J Biol Chem 1974;249:6910–6.

Identification of *AP2S1* Mutation and Effects of Low Calcium Formula in an Infant With Hypercalcemia and Hypercalciuria

Yasuko Fujisawa, Rie Yamaguchi, Eiichirou Satake, Konosuke Ohtaka, Toshiki Nakanishi, Keiichi Ozono, and Tsutomu Ogata

Department of Pediatrics (Y.F., R.Y., E.S., K.O., T.N., T.O.), Hamamatsu University School of Medicine, Hamamatsu 431–3192, Japan, and Department of Pediatrics (K.O.), Osaka University Graduate School of Medicine, Osaka 565–0871, Japan

Context: Although *AP2S1* has recently been shown to be a causative gene for familial hypocalciuric hypercalcemia type 3 (FHH3), knowledge about FHH3 remains poor.

Objective: Our objective was to report *AP2S1* mutation and effects of low calcium formula in a patient with hypercalcemia and hypercalciuria.

Patient: This Japanese female infant was found to have hypercalcemia by a routine laboratory test for poor weight gain on breast feeding. At 49 days of age, serum calcium (adjusted by Payne's formula) was 13.1 mg/dL, intact PTH 27 pg/mL, and urinary calcium-to-creatinine ratio 1.29 mg/mg. There was no evidence for hyperparathyroidism, PTHrP-producing neoplasm, and vitamin D excess. These data, except for hypercalciuria, appeared to be consistent with defective calcium-sensing receptor-mediated signaling. With use of low calcium formula containing 2.6 mg/dL of calcium, she showed catch-up growth, and serum calcium was decreased, as was urinary calcium-to-creatinine ratio. Furthermore, feeding with a mixture of low calcium formula and standard formula with a 2:1 ratio maintained serum calcium ~12 mg/dL without markedly increasing serum PTH.

Results: Although no pathologic mutation was detected in *CASR* or *GNA11*, a presumably de novo heterozygous mutation (p.Arg15Leu), a previously reported causative mutation for FHH3, was identified in *AP2S1* of this patient.

Conclusions: The results imply that lack of hypocalciuria does not necessarily argue against the presence of *AP2S1* mutations. The early infantile age of this patient would have played a certain role in the occurrence of hypercalciuria, and low calcium formula is worth attempting in infants with FHH. (***J Clin Endocrinol Metab* 98: E2022–E2027, 2013**)

Familial hypocalciuric hypercalcemia (FHH) is an autosomal-dominant disorder characterized by persistently increased serum calcium values and inappropriately low urinary calcium excretion, together with nonsuppressed serum PTH values (1). The term FHH is also conventionally applied to sporadic cases. FHH is classified into three types on the basis of chromosomal locations (3q21.1, 19p13.3, and 19q13.3) (2–5), and subsequent studies have shown that 1) FHH1 is caused by heterozygous loss-of-function mutations of *CASR* encoding calcium-sensing receptor (CASR) that belongs to the G protein-coupled receptor (GPCR) superfamily (6, 7); 2) FHH3

ISSN Print 0021-972X ISSN Online 1945-7197
Printed in U.S.A.

Received June 19, 2013. Accepted September 23, 2013.
First Published Online September 30, 2013

For editorial see page 4666

Abbreviations: AP2σ2, adaptor-related protein complex 2, sigma subunit; $[Ca^{2+}]_o$, extracellular calcium concentration; CASR, calcium-sensing receptor; FHH, familial hypocalciuric hypercalcemia; Gα11, G-protein subunit α_{11}; GPCR, G protein-coupled receptor; SNP, single-nucleotide polymorphism.

results from heterozygous mutations of *AP2S1* encoding adaptor-related protein complex 2, sigma subunit (AP2σ2) (8); and 3) FHH2 is due to heterozygous loss-of-function mutations of *GNA11* encoding G-protein subunit α_{11} (Gα11) (9). *CASR*, *AP2S1*, and *GNA11* mutations have been identified in ~65% of FHH patients, >20% of *CASR* mutation-negative FHH patients, and >10% of *CASR* and *AP2S1* mutation-negative FHH patients, respectively (1, 8, 9). CASR exists primarily on parathyroid chief cells and renal tubular cells and plays an essential role in calcium homeostasis, and Gα11 and AP2σ2 are involved in CASR-signaling (8, 9). Thus, FHH would primarily be ascribed to defective CASR-signal transduction in response to extracellular calcium concentration ($[Ca^{2+}]_o$).

For FHH3, it is notable that *AP2S1* mutations identified to date invariably affect the Arg15 residue (p.Arg15Cys, p.Arg15Leu, and p.Arg15His) (8). In this regard, calcium binding to CASR results in G protein-dependent stimulation, followed by CASR/β-arrestin/AP2 complex formation that is essential for clathrin-mediated endocytosis as well as for activation of G protein-independent pathways (8). Because the Arg15 residue of AP2σ2, a component of AP2, forms key contact with a dileucine motif of CASR, this would primarily explain why the Arg15 residue represents the mutation hot spot (8). Furthermore, functional studies using mutant AP2σ2 protein and CASR-expressing HEK293 cells have revealed 1) significantly higher EC_{50} values in the intracellular calcium concentration responses to changes in $[Ca^{2+}]_o$, which is indicative of decreased sensitivity to $[Ca^{2+}]_o$; and 2) significantly increased cell-surface localization of CASR after calcium stimulation, which is consistent with reduced CASR endocytosis (8). Because endocytosis plays a critical role in receptor recycling (ie, desensitization and resensitization) (10), defective endocytosis may be relevant to impaired sensitivity of CASR-expressing cells to $[Ca^{2+}]_o$.

To our knowledge, however, *AP2S1* mutations have been identified only in a few patients with FHH, and knowledge about FHH3 remains poor. Here, we report a heterozygous *AP2S1* mutation in a patient with hypercalcemia accompanied by hypercalciuria rather than hypocalciuria at the initial examination and discuss urine calcium excretion and clinical effects of low calcium formula.

Case Report

This Japanese female infant was born at 38 weeks of gestation after an uncomplicated pregnancy and delivery. Her birth length was 48.0 cm (±0 SD), her birth weight 2.7 kg (−0.6 SD), and her head circumference 33 cm (±0 SD).

At 41 days of age, she was seen at a local hospital due to poor sucking, constipation, and poor weight gain and was referred to us at 49 days of age because of hypercalcemia that was identified by a routine laboratory test. She was fed with breast milk with an average calcium concentration of ~25 mg/dL. Physical examination showed a somewhat feeble infant with no dysmorphic features. Her length was 50.9 cm (−2.1 SD), and her weight 3.7 kg (−2.0 SD). Biochemical data are summarized in Table 1 (because of low serum albumin, serum calcium values were adjusted by the Payne's formula: adjusted calcium [mg/dL] = calcium [mg/dL] − albumin [g/dL] + 4.0, which has been derived from the regression equation of calcium on albumin) (11). Bone survey was apparently normal, with no signs of osteolysis, osteopenia, or osteosclerosis (Supplemental Figure 1, published on The Endocrine Society's Journals Online web site at **Error! Hyperlink reference not valid.**). Ultrasound studies revealed no nephrocalcinosis. Chest and abdominal computed tomography showed no tumor-like mass lesion. Scintigraphy with 99mTc-methoxyisobutylisonitrile delineated four parathyroid glands with a similar intensity. Thus, she was found to have hypercalcemia, hypercalciuria, and inappropriately normal PTH value, as well as hypophosphatemia, high alkaline phosphatase, low 25-(OH)-vitamin D, and hypermagnesemia.

Her clinical course is summarized in Figure 1A. Intravenous infusion was immediately started with 0.9% saline solution. In addition, because her breast milk intake assessed by weight change before and after feeding was insufficient (~100 mL/kg/d), standard formula with a calcium concentration of 50 mg/dL was added from 50 days of age and, subsequently, she was fed by standard formula alone from 59 days of age because of gradual decrease in breast milk production. She was also treated with prednisolone and elcatonin (calcitonin derivative), together with drip infusion. Despite such treatments, her serum calcium remained high, and she manifested hypercalcemic symptoms such as insufficient sucking (daily formula intake, ~100 mL/kg/d) and constipation. Her growth remained compromised after admission, with a weight of 4.2 kg (−2.5 SD) at 72 days of age.

Thus, low calcium formula with a calcium concentration of 2.6 mg/dL was started at 72 days of age. Consequently, the adjusted serum calcium value gradually decreased to 11–12 mg/dL, and urinary calcium-to-creatinine ratio also decreased to a low to low-normal level (<0.1). Furthermore, her clinical condition improved promptly with sufficient daily formula intake (~160 mL/kg/d), and drip infusion was discontinued. However, this

Table 1. Summary of Biochemical Data

	Patient					
Age	**49 d**	**175 d**	**Normal Range**	**Father, 33 y**	**Mother, 34 y**	**Normal Range**
Serum						
Calcium (corrected), mg/dL	13.1	11.9	(9.0–11.0)	9.2	9.2	(8.8–10.2)
Inorganic phosphate, mg/dL	3.5	4.9	(4.8–7.5)	3.5	4.1	(2.5–4.5)
Alkaline phosphatase, mIU/mL	2226	1512	(500–1600)	N.E.	N.E.	
Intact PTH, pg/dL	27	97	(10–65)	25	50	(14–55)
PTHrP, pmol/L	<1.1	N.E.	(<1.1)	N.E.	N.E.	
25-(OH)-vitamin D, ng/mL	14	24	(7–40)	N.E.	N.E.	
1,25-$(OH)_2$-vitamin D, pg/mL	99	N.E.	(15–90)	N.E.	N.E.	
Calcitonin, pg/mL	59	N.E.	(15–86)	N.E.	N.E.	
Magnesium, mg/dL	2.4	2.9	(1.8–2.2)	N.E.	N.E.	
Urine				N.E.	N.E.	
Calcium/creatinine, mg/mg	1.29	0.10	(0.03–0.86)[a]	0.03	0.05	(<0.25)
Fractional excretion of calcium, %	2.5	0.12	(<2)[b]	N.E.	N.E.	
Tubular reabsorption of phosphate, %	>99	93	(78–97)	N.E.	N.E.	

Abbreviation: N.E., not examined.

Calcium intake of this patient is ~25 mg/kg/d at 49 d of age and 30 mg/kg/d at 175 d of age.

The values in the parentheses indicate age-matched normal range.

[a] The upper value (0.86) is the 95%ile level in infants aged <7 months (13).

[b] The value below 1% is the hallmark of FHH in adults (1).

Conversion factor to the SI unit: 0.25 for calcium (mmol/L), 0.32 for inorganic phosphate (mmol/L), 1.0 for alkaline phosphatase (IU/L), 0.106 for intact PTH (pmol/L), 2.50 for 25-(OH)-vitamin D (nmol/L), 2.40 for 1,25-$(OH)_2$-vitamin D (pmol/L), 1.0 for calcitonin (ng/L), and 0.41 for magnesium (mmol/L).

treatment resulted in markedly high serum PTH and alkaline phosphatase values, although skeletal findings remained apparently unremarkable at 132 days of age (Supplemental Figure 1). Thus, we modified the amount of oral calcium intake by mixing the low calcium formula and the standard formula. Consequently, feeding with a mixture of low calcium formula and standard formula with a 2:1 ratio containing ~18 mg/dL of calcium (the amount of oral calcium intake: ~30 mg/kg/d by taking ~160 mL/kg/d of formula) maintained the adjusted serum calcium value ~12 mg/dL, while avoiding a markedly high serum PTH value. On the last examination at 175 days of age, she showed catch-up growth with a length of 62.0 cm (−1.8 SD), a weight of 5.8 kg (−1.9 SD), and a head circumference of 42.2 cm (±0 SD), and biochemical data were restored toward normal (Table 1).

The nonconsanguineous parents were healthy, with normal biochemical data (Table 1). The elder sister was also clinically normal.

Mutation analysis

Because the clinical data, except for the initial hypercalciuria, were grossly consistent with defective CASR-mediated signaling (1, 8, 9), we examined all the coding exons and their flanking splice sites of *CASR*, *AP2S1*, and *GNA11*, using leukocyte genomic DNA samples. The primers used were as reported previously (8, 9, 12). This study was approved by Institutional Review Board Committee at Hamamatsu University School of Medicine and was performed after obtaining written informed consent.

Sequencing analysis identified a heterozygous missense mutation (c.44G>T, p.Arg15Leu) at exon 2 of *AP2S1* in this patient (Figure 1B). This mutation was absent from the parents and the elder sister, and restriction enzyme analysis and wild-type and mutant allele-specific amplification for the *AP2S1* mutation revealed no trace of mosaicism in the parents (Supplemental Figure 2). By contrast, no pathologic mutation was detected in *CASR* or *GNA11*. Furthermore, several single-nucleotide polymorphisms (SNPs) were identified, including *CASR* p.Arg990Gly (rs1042636) that was present in a heterozygous condition in the patient and the parents (Supplemental Table 1). The results of microsatellite genotyping were consistent with paternity and maternity of the parents (Supplemental Table 2).

Discussion

We identified p.Arg15Leu mutation of *AP2S1* in this infant. Because the p.Arg15Leu has been demonstrated as a

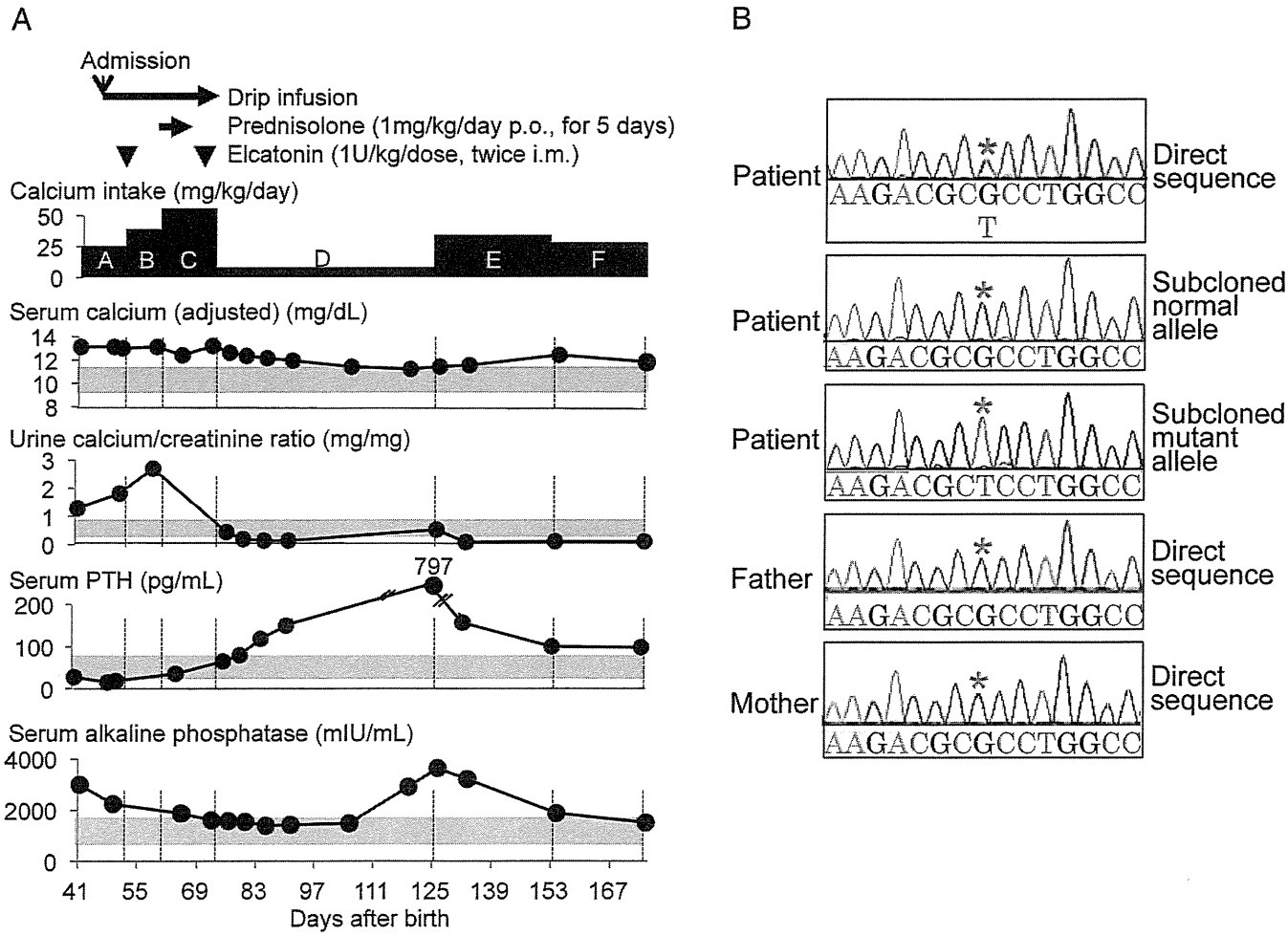

Figure 1. Clinical and molecular findings of this patient. Panel A, Clinical course of this patient. The data before admission have been measured at the previous local hospital. The gray areas indicate age-matched normal ranges. A: Breast milk, calcium intake ~25 mg/kg/d (calcium concentration, ~25 mg/dL; sucking volume, ~100 mL/kg/d). B: Breast milk plus standard formula (~1:1), calcium intake ~40 mg/kg/d (calcium concentration, ~40 mg/dL; sucking volume, ~100 mL/kg/d). C: Standard formula, calcium intake ~50 mg/kg/d (calcium concentration, 50 mg/dL; sucking volume, ~100 mL/kg/d). D: Low calcium formula, calcium intake ~4.2 mg/kg/d (calcium concentration, 2.6 mg/dL; sucking volume, ~160 mL/kg/d). E: Low calcium formula: standard formula = 1:1, calcium intake ~42 mg/kg/d (calcium concentration, 26.3 mg/dL; sucking volume, ~160 mL/kg/d). F: Low calcium formula: standard formula = 2:1, calcium intake ~29 mg/kg/d (calcium concentration, 18.4 mg/dL; sucking volume, ~160 mL/kg/d). Panel B, Electrochromatograms showing a heterozygous missense mutation of *AP2S1* (c.G44T, p.Arg15Leu) in this patient (indicated with asterisks). In addition to direct sequencing, sequencing has also been performed for normal and mutant alleles in this patient, after subcloning with TOPO TA Cloning Kit (Life Technologies).

causative mutation for FHH3 (8), this patient would also be diagnosed as having FHH3 in terms of the responsible gene. In addition, while parental somatic mutation involving germline but not leukocytes would remain possible, molecular data of this family argue for a de novo occurrence of this mutation.

Notably, this infant lacked hypocalciuria characteristic of FHH at the initial examination. This may primarily be ascribed to the early infantile age of this patient, because urine calcium excretion is high in (early) infancy and decreases with age (13, 14). Indeed, urine calcium excretion was higher in the initial period when the patient took ~25 mg/kg/d of calcium through breast feeding than in the recent period when she took ~30 mg/kg/d of calcium through formula feeding. However, apparent hypocalciuria has been described in a neonate with the same heterozygous p.Arg15Leu mutation and hypercalcemia (8), and apparent hypercalciuria has been reported in a neonate with a heterozygous inactivating mutation of *CASR* and hypercalcemia (15). Thus, infantile hypercalciuria would not be characteristic of FHH3 and may occur in a substantial fraction of FHH patients in the presence of hypercalcemia of a certain degree. In addition, hypercalciuria has exceptionally been documented in a few adult FHH patients of unknown type (16). In this regard, biochemical data of this patient may suggest the presence of mild vitamin D deficiency, although there was no discernible abnormality of radiological findings. Furthermore,

this patient had a heterozygous *CASR* p.Arg990Gly SNP with a gain-of-function effect (17) that may constitute a susceptibility factor for hypercalciuric hypocalcemia, although the parents heterozygous for this SNP had no abnormal findings. There would also be various hidden factors related to calcium homeostasis. Such diversity in multiple genetic and environmental factors, together with the effects of pathologic mutations, would be relevant to the variation in calcium-related biochemical data including urine calcium excretion among FHH patients.

Low calcium formula was given to this infant. This management not only reduced serum calcium value, but also ameliorated hypercalcemia-related clinical symptoms such as poor sucking, thereby permitting catch-up growth. Furthermore, although this management resulted in markedly increased PTH and alkaline phosphatase values, modification of the oral calcium intake mitigated such biochemical data without reoccurrence of clinical symptoms. Thus, low calcium formula with an appropriate mixture of standard formula is recommended as a therapeutic option in infantile patients with FHH.

Several findings would also be worth pointing out in this patient. First, aberrant calcium homeostasis was the sole discernible clinical phenotype in this patient, despite AP2σ2 being involved in signal transductions via multiple GPCRs other than CASR (8). This would provide further support for the notion that AP2σ2 plays a specific role in CASR-signaling (8). Second, although adjusted serum calcium value of ~12 mg/dL served to ameliorate clinical symptoms and biochemical values, serum PTH remained above the normal range. Such high serum PTH, although it is apparently uncommon in FHH1 and FHH2, may not be uncommon in FHH3 (especially in aged patients) (1, 9, 18), whereas hypocalciuria is shared by FHH1–3 (1, 8, 9). Thus, AP2σ2 might have distinctive effects on parathyroid function, although such a possible tissue-specific effect awaits further investigations. Third, hypermagnesemia was identified. Because hypermagnesemia is also identified in FHH1 and FHH2 (1, 9), this would be consistent with a positive role of CASR-signal transduction in magnesium homeostasis (19).

In summary, the results imply that lack of hypocalciuria does not necessarily argue against the impaired CASR-signal transduction, especially in infancy, and that low calcium formula is worth attempting in infants with FHH.

Acknowledgments

We thank Dr Gen Nishimura, Department of Radiology, Tokyo Metropolitan Children's Medical Center, for critical comments on the radiological findings of this patient.

Address all correspondence and requests for reprints to: Dr Yasuko Fujisawa, Department of Pediatrics, Hamamatsu University School of Medicine, 1-20-1 Handayama, Higashi-ku, Hamamatsu 431-3192, Japan. E-mail: yasuko@hama-med.ac.jp.

This work was supported in part by Grant for Research on Intractable Diseases from the Ministry of Health, Labor, and Welfare (H24-048), by a Grant from the National Center for Child Health and Development (23A-1), and by Grant-in-Aid for Scientific Research on Innovative Areas (22132004) from the Ministry of Education, Culture, Sports, Science, and Technology.

Disclosure Summary: The authors declare no conflict of interest.

References

1. **Egbuna OI, Brown EM.** Hypercalcaemic and hypocalcaemic conditions due to calcium-sensing receptor mutations. *Best Pract Res Clin Rheumatol.* 2008;22:129–148.
2. **Chou YH, Brown EM, Levi T, et al.** The gene responsible for familial hypocalciuric hypercalcemia maps to chromosome 3q in four unrelated families. *Nat Genet.* 1992;1:295–300.
3. **Heath H 3rd, Jackson CE, Otterud B, Leppert MF.** Genetic linkage analysis in familial benign (hypocalciuric) hypercalcemia: evidence for locus heterogeneity. *Am J Hum Genet.* 1993;53:193–200.
4. **Lloyd SE, Pannett AA, Dixon PH, Whyte MP, Thakker RV.** Localization of familial benign hypercalcemia, Oklahoma variant (FBHOk), to chromosome 19q13. *Am J Hum Genet.* 1999;64:189–195.
5. **Nesbit MA, Hannan FM, Graham U, et al.** Identification of a second kindred with familial hypocalciuric hypercalcemia type 3 (FHH3) narrows localization to a <3.5 megabase pair region on chromosome 19q13.3. *J Clin Endocrinol Metab.* 2010;95:1947–1954.
6. **Pollak MR, Brown EM, Chou YH, et al.** Mutations in the human Ca(2+)-sensing receptor gene cause familial hypocalciuric hypercalcemia and neonatal severe hyperparathyroidism. *Cell.* 1993;75:1297–1303.
7. **Hannan FM, Nesbit MA, Zhang C, et al.** Identification of 70 calcium-sensing receptor mutations in hyper- and hypo-calcaemic patients: evidence for clustering of extracellular domain mutations at calcium-binding sites. *Hum Mol Genet.* 2012;21:2768–2778.
8. **Nesbit MA, Hannan FM, Howles SA, et al.** Mutations in AP2S1 cause familial hypocalciuric hypercalcemia type 3. *Nat Genet.* 2013;45:93–97.
9. **Nesbit MA, Hannan FM, Howles SA, et al.** Mutations affecting G-protein subunit α11 in hypercalcemia and hypocalcemia. *N Engl J Med.* 2013;368:2476–2486.
10. **Ferguson SS.** Evolving concepts in G protein-coupled receptor endocytosis: the role in receptor desensitization and signaling. *Pharmacol Rev.* 2001;53:1–24.
11. **Payne RB, Little AJ, Williams RB, Milner JR.** Interpretation of serum calcium in patients with abnormal serum proteins. *Br Med J.* 1973;4:643–646.
12. **Miyata I, Yoshikawa H, Kurokawa N, Kanno K, Hayashi Y, Eto Y.** A neonatal case of autosomal dominant hypoparatyroidism without mutation of the CASR gene. *Clin Pediatr Endocrinol.* 2008;17:17–22.
13. **Sargent JD, Stukel TA, Kresel J, Klein RZ.** Normal values for random urinary calcium to creatinine ratios in infancy. *J Pediatr.* 1993;123:393–397.
14. **Matos V, van Melle G, Boulat O, Markert M, Bachmann C, Guignard JP.** Urinary phosphate/creatinine, calcium/creatinine, and

magnesium/creatinine ratios in a healthy pediatric population. *J Pediatr*. 1997;131:252–257.
15. **Obermannova B, Banghova K, Sumník Z, et al.** Unusually severe phenotype of neonatal primary hyperparathyroidism due to a heterozygous inactivating mutation in the CASR gene. *Eur J Pediatr*. 2009;168:569–573.
16. **Pasieka JL, Andersen MA, Hanley DA.** Familial benign hypercalcaemia: hypercalciuria and hypocalciuria in affected members of a small kindred. *Clin Endocrinol (Oxf)*. 1990;33:429–433.
17. **Vezzoli G, Terranegra A, Arcidiacono T, et al.** R990G polymorphism of calcium-sensing receptor does produce a gain-of-function and predispose to primary hypercalciuria. *Kidney Int*. 2007;71:1155–1162.
18. **McMurtry CT, Schranck FW, Walkenhorst DA, et al.** Significant developmental elevation in serum parathyroid hormone levels in a large kindred with familial benign (hypocalciuric) hypercalcemia. *Am J Med*. 1992;93:247–258.
19. **Cole DE, Quamme GA.** Inherited disorders of renal magnesium handling. *J Am Soc Nephrol*. 2000;11:1937–1947.

IL-6 negatively regulates osteoblast differentiation through the SHP2/MEK2 and SHP2/Akt2 pathways in vitro

Shoichi Kaneshiro, Kosuke Ebina, Kenrin Shi, Chikahisa Higuchi, Makoto Hirao, Michio Okamoto, Kota Koizumi, Tokimitsu Morimoto, et al.

Journal of Bone and Mineral Metabolism

ISSN 0914-8779

J Bone Miner Metab
DOI 10.1007/s00774-013-0514-1

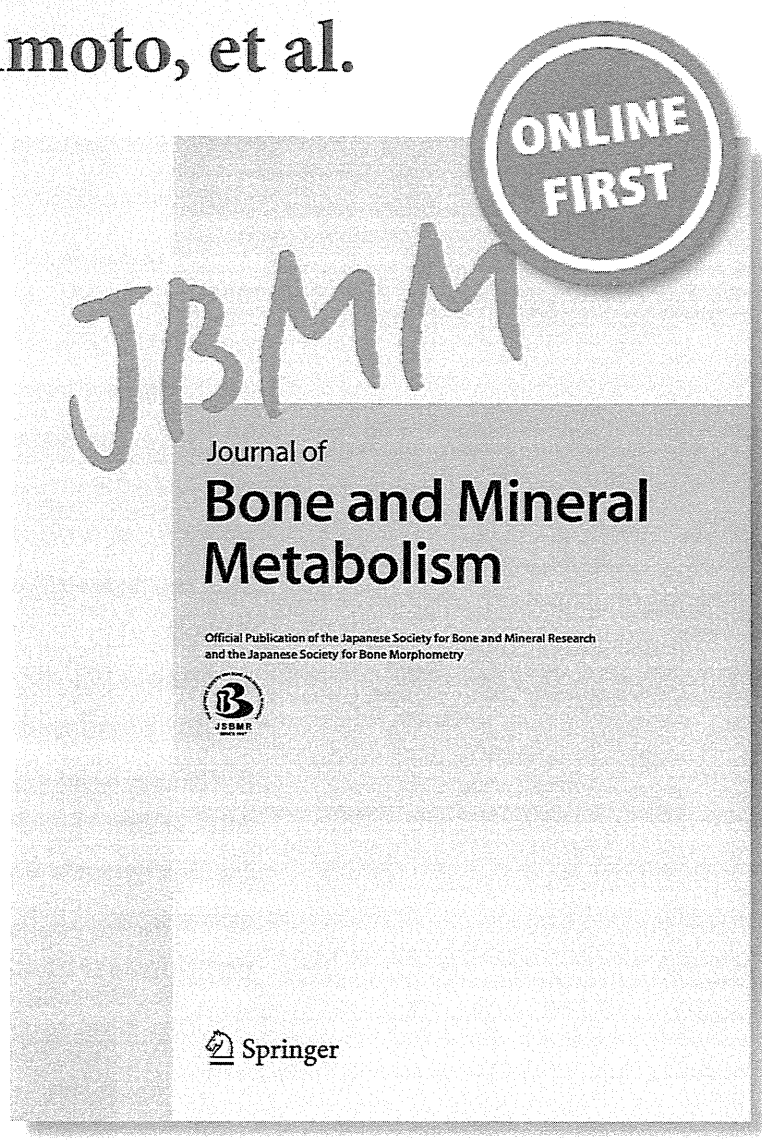

Springer

J Bone Miner Metab
DOI 10.1007/s00774-013-0514-1

ORIGINAL ARTICLE

IL-6 negatively regulates osteoblast differentiation through the SHP2/MEK2 and SHP2/Akt2 pathways in vitro

Shoichi Kaneshiro · Kosuke Ebina · Kenrin Shi · Chikahisa Higuchi · Makoto Hirao · Michio Okamoto · Kota Koizumi · Tokimitsu Morimoto · Hideki Yoshikawa · Jun Hashimoto

Received: 13 February 2013 / Accepted: 7 August 2013

Abstract It has been suggested that interleukin-6 (IL-6) plays a key role in the pathogenesis of rheumatoid arthritis (RA), including osteoporosis not only in inflamed joints but also in the whole body. However, previous in vitro studies regarding the effects of IL-6 on osteoblast differentiation are inconsistent. The aim of this study was to examine the effects and signal transduction of IL-6 on osteoblast differentiation in MC3T3-E1 cells and primary murine calvarial osteoblasts. IL-6 and its soluble receptor significantly reduced alkaline phosphatase (ALP) activity, the expression of osteoblastic genes (Runx2, osterix, and osteocalcin), and mineralization in a dose-dependent manner, which indicates negative effects of IL-6 on osteoblast differentiation. Signal transduction studies demonstrated that IL-6 activated not only two major signaling pathways, SHP2/MEK/ERK and JAK/STAT3, but also the SHP2/PI3K/Akt2 signaling pathway. The negative effect of IL-6 on osteoblast differentiation was restored by inhibition of MEK as well as PI3K, while it was enhanced by inhibition of STAT3. Knockdown of MEK2 and Akt2 transfected with siRNA enhanced ALP activity and gene expression of Runx2. These results indicate that IL-6 negatively regulates osteoblast differentiation through SHP2/MEK2/ERK and SHP2/PI3K/Akt2 pathways, while affecting it positively through JAK/STAT3. Inhibition of MEK2 and Akt2 signaling in osteoblasts might be of potential use in the treatment of osteoporosis in RA.

Keywords Interleukin-6 · Osteoblast differentiation · MEK2 · Akt2 · Signaling pathway

Introduction

Inflammation-mediated bone loss is a major feature of various bone diseases, including rheumatoid arthritis (RA). Interleukin-6 (IL-6) contributes to the development of arthritis and is present at high concentrations in the serum and synovial fluid of patients with RA [1–4]. Soluble IL-6 receptor (sIL-6R) is also elevated in the serum and synovial fluid of RA patients [5, 6], and IL-6 exerts its action by binding either to its membrane-bound receptor (mIL-6R) or to sIL-6R. Moreover, IL-6 is closely associated with the expression of receptor activator of NF-κB ligand (RANKL) in osteoblasts [7]. That is to say, IL-6 acts indirectly on osteoclastogenesis by stimulating the release of RANKL by cells within bone tissues such as osteoblasts [8]. It can unquestionably be said that IL-6 plays a major role in the pathogenesis of RA [9–12], including osteoporosis not only in inflamed joints but also in the whole body.

There have been several studies on the effect of IL-6 on bone turnover in animal models. In IL-6 knock-out mice,

Electronic supplementary material The online version of this article (doi:10.1007/s00774-013-0514-1) contains supplementary material, which is available to authorized users.

S. Kaneshiro · K. Ebina (✉) · K. Shi · C. Higuchi · M. Okamoto · K. Koizumi · T. Morimoto · H. Yoshikawa
Department of Orthopaedic Surgery, Graduate School of Medicine, Osaka University, 2-2 Yamadaoka, Suita, Osaka 565-0871, Japan
e-mail: k-ebina@umin.ac.jp

M. Hirao
Department of Orthopaedic Surgery, Osaka Minami Medical Center, National Hospital Organization, 2-1 Kidohigashi, Kawachinagano, Osaka 586-8521, Japan

J. Hashimoto
Department of Rheumatology, Osaka Minami Medical Center, National Hospital Organization, 2-1 Kidohigashi, Kawachinagano, Osaka 586-8521, Japan

Published online: 12 October 2013

microstructure abnormalities in cortical bones and delayed fracture healing were observed [13, 14], in spite of the evident normal phenotype [15]. Also, bone loss after estrogen depletion was mitigated in IL-6-deficient mice, while a high level of IL-6 and bone loss are seen in wild-type mice [13]. Moreover, IL-6-overexpressed-transgenic mice develop osteopenia and defective ossification, in which the activity of mature osteoblasts is significantly decreased [16]. All these findings, together with studies on human RA patients [17, 18], indicate that IL-6 plays a major role in bone turnover and is an important regulator of bone homeostasis.

Recently, several biological agents have been introduced for the treatment of RA and have demonstrated not only potent anti-inflammatory effects but also inhibitory effects on joint destruction. Among these biological agents, tocilizumab, an anti-IL-6 receptor antibody, has been reported to increase serum bone formation markers in RA patients [19], suggesting that IL-6 has a negative effect on osteoblast differentiation. However, previous reports regarding the effects of IL-6 on osteoblast differentiation in vitro have been inconsistent [20]. IL-6 has been shown to decrease the expression of differentiation markers in osteoblasts [21, 22] and to inhibit bone formation [23], while it has been shown to induce osteoblast differentiation [24, 25].

Binding of IL-6 with sIL-6R or mIL-6R leads to subsequent homodimerization of the signal-transducing molecule gp130, followed by activation of two major intracellular signaling pathways, Janus protein tyrosine kinase (JAK)/signal transducer and activator of transcription factors (STAT) 3, or Src-homology domain 2 containing protein-tyrosine phosphatase (SHP2)/mitogen-activated protein kinase-extracellular signal–regulated kinase kinase (MEK)/mitogen-activated protein kinase (MAPK), also called extracellular signal-regulated kinase (ERK) [26]. There have been many reports in which the effects of IL-6 on JAK/STAT3 and SHP2/ERK signal transduction pathways have been studied in osteoblasts, though it is still controversial whether differentiation is enhanced by IL-6 [9, 20]. SHP2 can also form a tertiary complex with the scaffolding proteins Gab1/2 and the p85 subunit of phosphatidylinositol-3-kinase (PI3K) [27], which leads to activation of the Akt pathway. Several papers have so far reported that the PI3K/Akt pathway triggered by IL-6 plays important roles in various cells [28–32], but no reports have been published regarding the effect of IL-6 on this pathway in osteoblasts.

The purpose of this study was to clarify the effect of IL-6 on osteoblast differentiation in vitro, with consideration of intracellular signaling pathways in murine MC3T3-E1 osteoblastic cells and primary murine calvarial osteoblasts.

Materials and methods

Ethics statement

Prior to the study, all experimental protocols were approved by the Ethics Review Committee for Animal Experimentation of Osaka University School of Medicine.

Cell culture

MC3T3-E1 osteoblastic cells were purchased from Riken Cell Bank (Tsukuba, Japan). MC3T3-E1 cells were cultured in α-minimum essential medium (α-MEM) containing 10 % fetal bovine serum (FBS; Equitech-Bio, Kerrville, TX, USA) and 1 % penicillin and streptomycin at 37 °C in a humidified atmosphere of 5 % CO_2. All media were purchased from Life Technologies Japan (Tokyo, Japan). Murine primary osteoblasts were isolated from the calvariae of 3-day-old C57BL/6 mice (Charles River Laboratories Japan, Inc, Osaka, Japan) by sequential collagenase digestion as described previously [33].

MC3T3-E1 cells and murine calvarial osteoblasts were seeded at 1×10^5 cells per well in 12-well plates. After the cells reached confluence, the medium was replaced to induce osteoblast differentiation. The differentiation medium contained 10 % FBS, 10 mM β-glycerophosphate, and 50 μg/ml ascorbic acid in the absence or presence of recombinant mouse (rm) IL-6 (R&D Systems, Inc., Minneapolis, MN, USA) (10, 50 ng/mL), and rm sIL-6R (R&D Systems) (100 ng/mL). The medium and reagents were renewed every 3 days.

To study signal transduction, the following inhibitors or vehicle (DMSO) (Sigma-Aldrich, St.Louis, MO, USA) were added to culture medium at several concentrations; MEK inhibitor (U0126; 1, 2.5, 5 μM; Cell Signaling Technology, Danvers, MA, USA), STAT3 inhibitor (V Stattic; 2.5, 5 μM; Calbiochem, La Jolla, CA, USA), PI3K inhibitor (LY294002; 1, 2.5, 5 μM; Cell Signaling Technology), and SHP2 inhibitor (PHPS1; 5, 20, 40 μM; Sigma-Aldrich). These inhibitors were added 1 h before treatment with IL-6/sIL-6R. All inhibitors were maintained until the end of the culture period at the indicated concentrations.

Alkaline phosphatase (ALP) staining and activity

MC3T3-E1 cells and murine calvarial osteoblasts were treated with or without IL-6/sIL-6R and signal pathway inhibitors after the cells reached confluence and were incubated for 6 days.

For ALP staining, after fixation with 10 % formalin, cells were washed twice with phosphate-buffered saline (PBS) (pH 7.4) and incubated with ALP substrate solution,

0.1 mg/ml naphthol AS-MX (Sigma-Aldrich), and 0.6 mg/ml fast violet B salt (Sigma-Aldrich) in 0.1 M Tris–HCl (pH 8.5) for 20 min.

To measure ALP activity, cells were washed twice with PBS and lysed in Mammalian Protein Extraction Reagent (Pierce, Rockford, IL, USA) according to the manufacturer's protocol. ALP activity was assayed using *p*-nitrophenylphosphate as a substrate by an Alkaline Phosphatase Test Wako (Wako Pure Chemicals Industries, Ltd., Osaka, Japan), and the protein content was measured using the Bicinchoninic Acid Protein Assay Kit (Pierce).

Proliferation assay

MC3T3-E1 cells were cultured in 96-well plates at a concentration of 2.0×10^4 cells/cm^2 in α-MEM containing 10 % FBS. Cells were incubated for 1 day, after which the medium was treated with IL-6/sIL-6R for 3 days. Cell proliferation was assessed using the Premix WST-1 Cell Proliferation Assay System (Takara Bio, Inc., Otsu, Japan) according to the manufacturer' s instructions. We performed this assay every 24 h.

Alizarin red staining

After fixation with 10 % formalin, MC3T3-E1 cells and murine calvarial osteoblasts were washed with distilled water, and stained with alizarin red S solution (Sigma-Aldrich) (pH 6.0) for 10 min, followed by incubation in 100 mM cetylpyridinium chloride for 1 h at room temperature to dissolve and release calcium-bound alizarin red. The absorbance of the released alizarin red was then measured at 570 nm [34]. To measure the value of absorbance for alizarin red, the absorbance data were normalized by total DNA content. Total DNA was extracted using a DNeasy Blood & Tissue Kit (Qiagen, Düsseldorf, Germany).

Knockdown of MEK1, MEK2, Akt1 and Akt2 using RNA interference

MC3T3-E1 cells were transfected with small interfering RNAs (siRNA) using Lipofectamine RNAiMAX (Life Technologies Japan) according to the reverse transfection method in the manufacturer's protocol.

The siRNAs for MEK2, Akt1 and Akt2 and that for MEK1 were purchased from Cell Signaling Technology and Qiagen, respectively, with negative controls for each molecule. MC3T3-E1 cells transfected with siRNA were seeded in 24-well plates at a concentration of 1.0×10^4 cells/cm^2 for 48 h. The medium was then replaced with differentiation medium with vehicle or with 20 ng/ml IL-6 and 100 ng/ml sIL-6R and the cells were incubated for 3 days prior to use for further experiments.

Western blotting

Cells cultured in 6-well plates for 2 days were washed twice with PBS and then homogenized with 100 μl of Kaplan buffer (150 mM NaCl, 50 mM Tris–HCL pH 7.4, 1 % NP40, 10 % glycerol, and 1 tablet per 50 ml buffer of protease inhibitor cocktail and phosphatase inhibitor cocktail). The lysates were centrifuged at 13,000 rpm for 20 min at 4 °C, and the supernatants were used for electrophoresis after a protein assay using bovine serum albumin as standard. Western blotting was performed by use of the following antibodies purchased from Cell Signaling Technology, except for phosphate anti-Akt2 antibody from Enogene Biotech (New York, NY, USA): phosphate anti-STAT3 (Tyr705) (1:2000) and anti-STAT3 (1:1000); phosphate anti-Akt (Ser473) (1:2000), phosphate anti-Akt2 (Ser474) (1:1000), anti-Akt1, anti-Akt2, and anti-Akt (1:1000); phosphate anti-ERK (Thr202/Tyr204) (1:2000), anti-MEK1, anti-MEK2 and anti-ERK (1:1000); and phosphate anti-SHP2 (Tyr542) (1:1000). To control for protein loading, blots were additionally stained with anti-β actin antibody (1:1000).

Reverse transcription polymerase chain reaction (RT–PCR)

Total RNA was extracted from cells with an RNeasy Mini Kit (Qiagen), and first-strand cDNA was synthesized using SuperScript II RNase H-reverse transcriptase (Life Technologies Japan). Then PCR was performed using Ex Taq (Takara Bio) and the following primers:

Osteocalcin (forward primer 5′-CTCACTCTGCTGGCCCTG-3′; reverse primer 5′-CCGTAGATGCGTTTGTAGGC-3′);
Osterix (forward primer 5′-AGGCACAAAGAAGCCATAC-3′; reverse primer 5′-AATGAGTGAGGGAAGGGT-3′);
Runx2 (forward primer 5′-GCTTGATGACTCTAAACCTA-3′; reverse primer 5′-AAAAAGGGCCCAGTTCTGAA-3′);
GAPDH (forward primer 5′-TGAACGGGAAGCTCACTGG-3′; reverse primer 5′-TCCACCACCCTGTTGCTGTA-3′).

Quantitative real-time PCR analysis

We obtained cDNA by reverse transcription as mentioned above, and proceeded with real-time PCR using a Light Cycler system (Roche Applied Science, Basel, Switzerland). The SYBR Green assay using a Quantitect SYBR Green PCR Kit (Qiagen), in which each cDNA sample was evaluated in triplicate 20-μl reactions, was used for all

target transcripts. Expression values were normalized to GAPDH.

Statistical analysis

The results are expressed as the mean ± standard error (SE). Between-group differences were assessed using the ANOVA test. A probability value of <0.05 was considered to indicate statistical significance.

Results

IL-6/sIL-6R does not affect proliferation, but significantly reduces ALP activity and expression of osteoblastic genes in MC3T3-E1 cells

We first measured the proliferation of MC3T3-E1 cells with IL-6. Cell proliferation did not show significant difference in any culture condition (Fig. 1a).

To investigate the influence of IL-6 treatment on osteoblast differentiation, we examined ALP activity in MC3T3-E1 cells. As shown in Fig. 1b and c, IL-6/sIL-6R significantly reduced ALP activity in a dose-dependent manner. The single addition of sIL-6R did not show a significant difference as compared to the negative control with vehicle. As shown in Fig. 1d and e, gene expression of Runx2, osterix and osteocalcin was significantly downregulated by IL-6/sIL-6R in a dose-dependent manner. Again, the single addition of sIL-6R did not show significant difference as compared to the negative control with vehicle.

IL-6/sIL-6R significantly inhibits mineralization of extracellular matrix (ECM) in MC3T3-E1 cells

As shown in Fig. 2a, IL-6/sIL-6R significantly inhibited the mineralized area in a dose-dependent manner. The single addition of sIL-6R did not show a significant difference as compared to the negative control with vehicle (Fig. 2a). Quantitative analysis of mineralization by measuring the absorbance of alizarin red revealed a significant decrease by IL-6/sIL-6R in a dose-dependent manner (Fig. 2b).

IL-6/sIL-6R activates ERK, STAT3 and Akt2 signal transduction pathways in MC3T3-E1 cells

When MC3T3-E1 cells were incubated in the presence of IL-6/sIL-6R, phosphorylation of ERK, STAT3 and Akt was clearly observed at 15 min, and their activation became weaker at 30 min. When only sIL-6R was added, there was no apparent activation of ERK, STAT3, or Akt as compared to the negative control (Fig. 3a). As for Akt, the phosphorylation by IL-6/sIL-6R was recognized more strikingly as early as 5 min in a dose-dependent manner, both for whole and for Akt2 only, one of its three isoforms (Fig. 3b).

IL-6-induced activation of ERK is enhanced by blocking the STAT3 signaling pathway, and IL-6-induced ERK and Akt signaling pathways negatively regulate each other reciprocally

The SHP2 inhibitor PHPS1 [35] inhibited IL-6-induced phosphorylation of ERK and Akt to the constitutive level, but did not inhibit STAT3 (Fig. 4a and Supplementary Fig. S1a), suggesting that the downstream pathways of SHP2 are ERK and Akt, not STAT3. The STAT3 inhibitor V Stattic inhibited the phosphorylation of STAT3 but enhanced ERK significantly (Fig. 4a and Supplementary Fig. S1a), suggesting that STAT3 could negatively regulate ERK, which is consistent with previous reports [36]. The MEK/ERK inhibitor U0126 completely inhibited both constitutive and IL-6-induced phosphorylation of ERK but enhanced those of Akt. Moreover, the PI3K/Akt inhibitor LY294002 completely inhibited both constitutive and IL-6-induced phosphorylation of Akt but enhanced those of ERK (Fig. 4b and Supplementary Fig. S1b). From these findings, we concluded that IL-6-induced ERK and Akt signaling pathways, both of which are downstream of SHP2, can negatively regulate each other reciprocally.

The negative effects of IL-6 on osteoblast differentiation are restored by inhibition of MEK, PI3K and SHP2, while they are enhanced by inhibition of STAT3

To identify the intracellular signaling pathways associated with the downregulation of osteoblast differentiation, the effects of various signal transduction inhibitors, consisting of a MEK inhibitor (U0126), PI3K inhibitor (LY294002), SHP2 inhibitor (PHPS1), and STAT3 inhibitor (V Stattic), were assessed for ALP activity, the expression of osteoblastic genes (Runx2, osterix and osteocalcin), and the mineralization of ECM.

The negative effect of IL-6/sIL-6R on ALP activity was restored by treatment with either U0126, LY294002, or PHPS1 in a dose-dependent manner. On the other hand, the negative effect of IL-6/sIL-6R on ALP activity was enhanced by treatment with V Stattic (Fig. 5a). These results indicate that the SHP2-associated signal transduction molecules MEK/ERK and PI3K/Akt have a negative effect on osteoblast differentiation, whereas the JAK-associated molecule STAT3 has a positive effect.

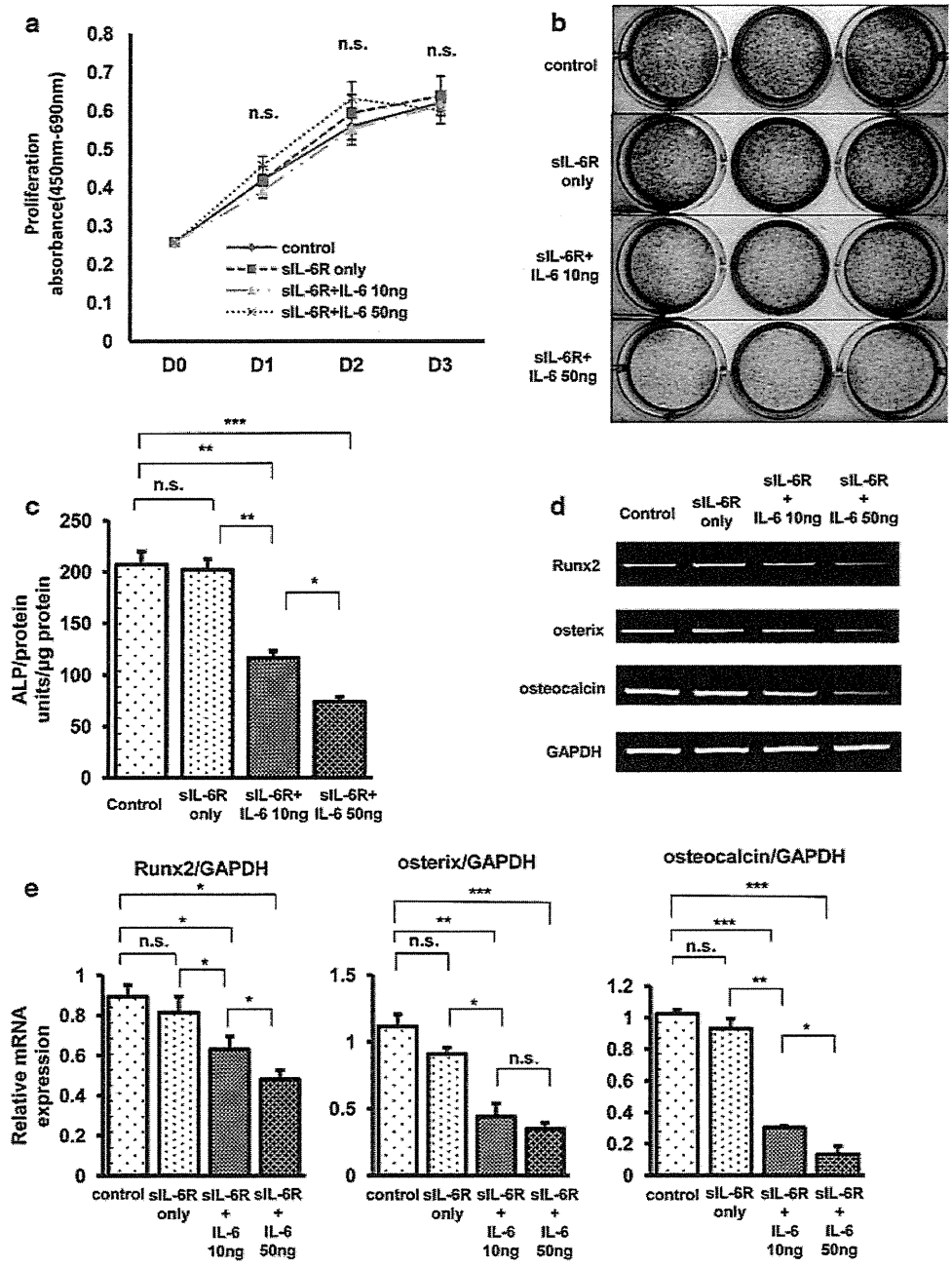

Fig. 1 IL-6/sIL-6R significantly reduced ALP activity and expression of osteoblastic genes in MC3T3E1 cells, but did not affect proliferation. **a** Proliferation of MC3T3-E1 cells with IL-6/sIL-6R was examined. Cells were pre-incubated for 1 day and then the medium was treated with or without IL-6/sIL-6R for 3 days. Cell proliferation assay was performed daily throughout the 4 days of incubation. Cell proliferation did not show significant differences in any culture condition. **b** ALP staining was performed in MC3T3-E1 cells treated with or without IL-6/sIL-6R for 6 days. Apparently significant reduction of ALP staining was recognized in cells treated with either 10 or 50 ng/ml IL-6. **c** ALP activity of the lysates of MC3T3-E1 cells treated with or without IL-6/sIL-6R for 6 days was measured using p-nitrophenylphosphate as a substrate. IL-6/sIL-6R significantly reduced ALP activity in a dose-dependent manner. **d** Total RNA was extracted from MC3T3-E1 cells treated with or without IL-6/sIL-6R for 6 days and subjected to RT-PCR for osteoblastic genes Runx2, osterix, and osteocalcin. Apparently significant reduction of osteoblastic gene expression was recognized in cells treated with either 10 or 50 ng/ml IL-6. **e** Real-time PCR for Runx2, osterix, and osteocalcin was performed for quantitative analysis. Data were normalized to GAPDH expression and are shown as the ratio of expression compared to control cells treated with vehicle. The expression of osteoblastic genes was significantly downregulated by IL-6/sIL-6R in a dose-dependent manner. Representative data from at least 3 independent experiments are shown. Data are shown as mean ± SE. *n.s.* not significant; $^{*}P < 0.05$; $^{**}P < 0.001$; $^{***}P < 0.001$

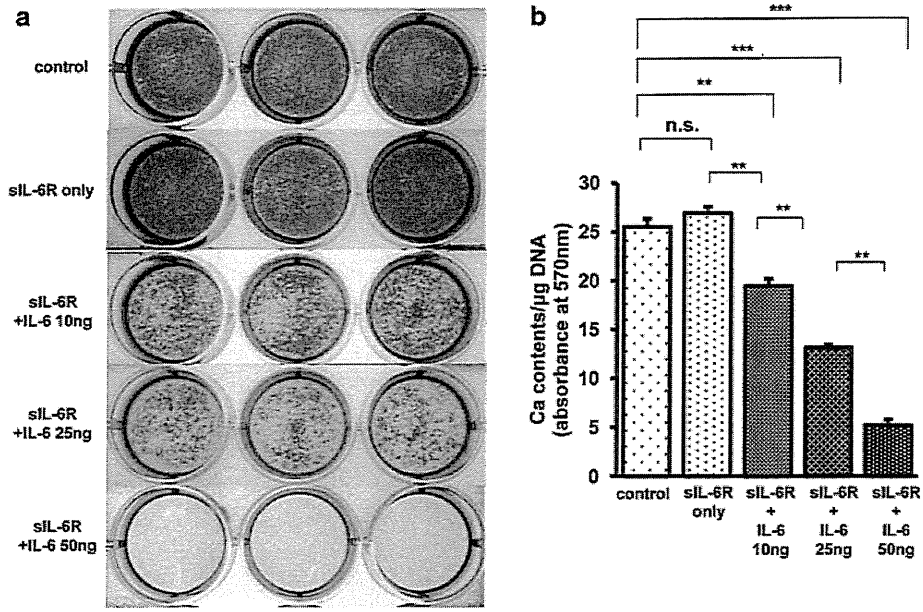

Fig. 2 IL-6/sIL-6R significantly inhibited the mineralization of ECM in MC3T3E1 cells. MC3T3-E1 cells were treated with or without IL-6/sIL-6R and were incubated for 21 days. **a** After fixation, the cells were stained with alizarin red solution. Apparently significant reduction of alizarin red staining was recognized in the cells treated with either 10, 25, or 50 ng/ml IL-6. **b** Matrix mineralization was quantified by the measurement of absorbance of alizarin red and normalized by total DNA content. Matrix mineralization was significantly reduced by IL-6/sIL-6R in a dose-dependent manner. Representative data from at least 3 independent experiments are shown. Data are shown as mean ± SE. *n.s.* not significant; $*P < 0.05$; $**P < 0.001$; $***P < 0.001$

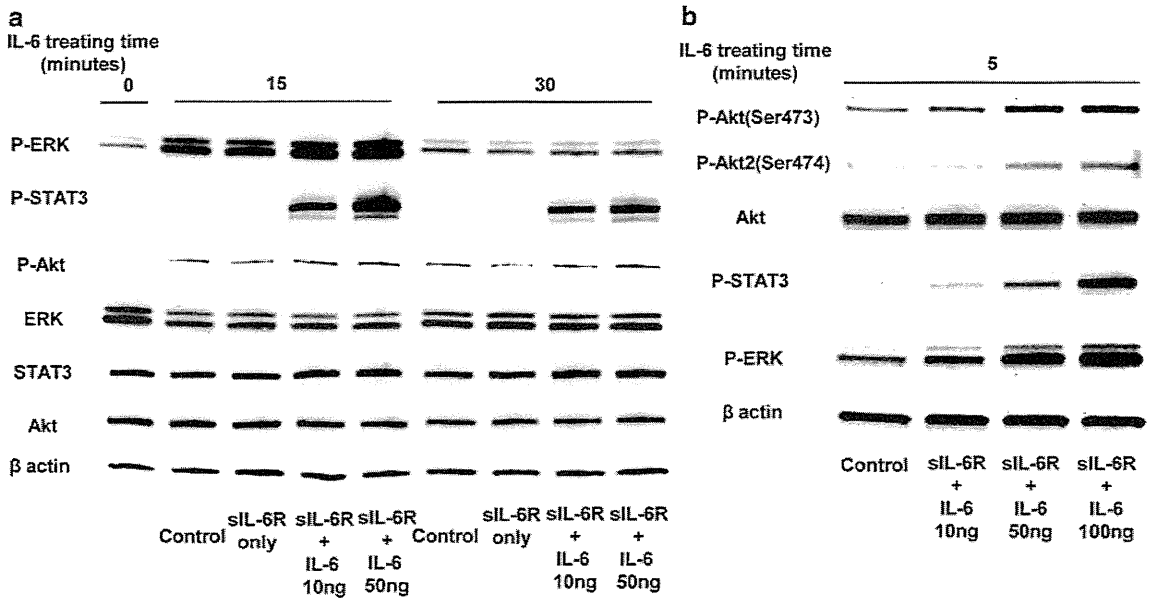

Fig. 3 IL-6/sIL-6R-activated ERK, STAT3, and Akt2 signal transduction pathways in MC3T3-E1 cells. **a** MC3T3-E1 cells were treated with vehicle or with 10 or 50 ng/ml IL-6 and 100 ng/ml sIL-6R in a time-course experiment (0, 15, and 30 min). Western blot analysis was performed using cell lysates for the detection of ERK, STAT3, and Akt, either phosphorylated or not. IL-6/sIL-6R significantly induced the phosphorylation of ERK, STAT3, and Akt in a dose-dependent manner. **b** MC3T3-E1 cells were incubated with increasing concentrations of IL-6 and 100 ng/ml sIL-6R for 5 min. Western blotting was performed using cell lysates for the detection of ERK, STAT3, as well as Akt, either non-phosphorylated, phosphorylated, or the phosphorylated isoform Akt2. The phosphorylation of both whole Akt and Akt2 by IL-6/sIL-6R was recognized more strikingly in a dose-dependent manner. Representative data from at least three independent experiments are shown